 Accepted Manuscript published as JOE-18-0493.R1. Accepted for publication: 30-Nov-2018

Title: High Glucose Alters Fetal Rat Islet Transcriptome and Induces Progeny Islet Dysfunction

Authors: Jose Casasnovas[1], Yunhee Jo[1], Xi Rao[2], Xiaoling Xuei[2], Mary E. Brown[3], Kok Lim Kua[1]

[1]Department of Pediatrics, Indiana University School of Medicine, Indianapolis, Indiana, United States. [2]Center for Medical Genomics, Department of Medical and Molecular Genetics, Indiana University School of Medicine, Indianapolis, Indiana, United States. [3]The Indiana Center for Biological Microscopy, Division of Nephrology, Indiana University School of Medicine, Indianapolis, Indiana, United States.

*JC and YJ contributed equally as co-first authors

Corresponding Author: Kok Lim Kua, MD

Indiana University School of Medicine

635, Barnhill Dr, MS2057

Indianapolis, IN 46202

email: kkua@iu.edu

phone: 317-274-4142

Keywords: Maternal hyperglycemia, fetal hyperglycemia, late gestation hyperglycemia, offspring of diabetic mothers, pancreatic islet programming, fetal islet transcriptome

Running Title/Short title: Fetal Hyperglycemia Induces Islet Hypofunction

Word count: 5250 words

Abstract

Offspring of diabetic mothers are susceptible to developing type 2 diabetes due to pancreatic islet dysfunction. However, the initiating molecular pathways leading to offspring pancreatic islet dysfunction are unknown. We hypothesized that maternal hyperglycemia alters offspring pancreatic islet transcriptome and negatively impacts offspring islet function. We employed an infusion model capable of inducing localized hyperglycemia in fetal rats residing in the left uterine horn, thus avoiding other factors involved in programming offspring pancreatic islet health. While maintaining euglycemia in maternal dams and right uterine horn control fetuses, hyperglycemic fetuses in the left uterine horn had higher serum insulin and pancreatic beta cell area. Upon completing infusion from GD20 to 22, RNA-sequencing was performed on GD22 islets to identify the hyperglycemia-induced altered gene expression. Ingenuity pathway analysis of the altered transcriptome found that diabetes mellitus and inflammation/cell death pathways were enriched. Interestingly, the down-regulated genes modulate more diverse biological processes, which includes responses to stimuli and developmental processes. Next, we performed *ex-* and *in-vivo* studies to evaluate islet cell viability and insulin secretory function in weanling and adult offspring. Pancreatic islets of weanlings exposed to late gestation hyperglycemia had decreased cell viability in basal state and glucose-induced insulin secretion. Lastly, adult offspring exposed to in-utero hyperglycemia also exhibited glucose intolerance and insulin secretory dysfunction. Together, our results demonstrate that late gestational hyperglycemia alters the fetal pancreatic islet transcriptome and increases offspring susceptibility to developing pancreatic islet dysfunction.

Accepted Manuscript published as JOE-18-0493.R1. Accepted for publication: 30-Nov-2018

INTRODUCTION

Diabetes complicates 5.6-11.7% of all pregnancies (Hunt & Schuller 2007; DeSisto 2014), with affected mothers and offspring vulnerable to adverse metabolic outcomes (Ratner *et al.* 2008; Fraser & Lawlor 2014; Tam *et al.* 2017; Das Gupta *et al.* 2018) . Offspring of diabetic mothers suffer a 4- to 8-fold increased risk of developing type 2 diabetes (Clausen *et al.* 2008) due to obesity (Raghavan *et al.* 2017), insulin resistance (Sauder *et al.* 2017), and pancreatic islet dysfunction (Gautier *et al.* 2001; Tam *et al.* 2017). In addition to increased adiposity, recent human studies have shown that by the age of seven, children born to diabetic mothers had impaired glucose tolerance and decreased beta cell compensation (Tam *et al.* 2017). Animal offspring exposed to a diabetic milieu *in-utero* also exhibited pancreatic islet dysfunction (Cerf *et al.* 2006; Han *et al.* 2007; Blondeau *et al.* 2011; Zambrano *et al.* 2016). While both human and animal studies confirmed that the altered *in-utero* environment during diabetic pregnancy permanently reprograms the metabolic health of offspring, the underlying mechanisms modulating offspring pancreatic islet function remain poorly understood.

During maternal diabetes (type 1, type 2, and gestational diabetes), maternal hyperglycemia occurs secondary to inadequate insulin secretion and/or underlying insulin resistance. Commonly used animal models simulating diabetic pregnancy, such as chemically-induced maternal diabetes (insulin deficiency model) (Han *et al.* 2007; Blondeau *et al.* 2011) or maternal high fat diet model (maternal insulin resistance/obesity) (Cerf *et al.* 2006, 2009; Zambrano *et al.* 2016), expose developing fetuses to a multitude of maternal biochemical changes far beyond hyperglycemia during critical development periods (Xiang *et al.* 2007; Wang *et al.* 2010). Maternal hyperglycemia has been implicated as the primary contributing factor (Clausen *et al.* 2008; Tam *et al.* 2017; Martin & Sacks 2018) and has been shown to induce pancreatic islet dysfunction early during fetal life (Frost *et al.* 2012; Green *et al.* 2012). However, the exact means by which maternal hyperglycemia impacts offspring metabolic health is unknown due to 1) the absence of a rodent model capable of exposing the developing fetus to

an exclusively excessive glucose supply, and 2) a limited understanding in early transcriptome changes induced by maternal hyperglycemia.

Both rodents and humans undergo continuous pancreatic beta cell mass expansion and functional maturation postnatally until young adulthood (Bonner-Weir *et al.* 2016). This process of postnatal pancreatic beta cell mass expansion and functional maturation is tightly regulated by transcription factors (eg. MafB, Ucn3) (Artner *et al.* 2007; van der Meulen & Huising 2014), miRNA (Jacovetti *et al.* 2015, 2017), and growth factors (insulin, INGAP) (Barbosa *et al.* 2006). Changes in any of these factors could affect the biological and mechanistic pathways involved with diabetes-induced pancreatic islet dysfunction in offspring.

The aim of this study was to identify early transcriptome changes induced by maternal hyperglycemia on pancreatic islets of offspring, uncovering a primary mechanism of offspring pancreatic islet programming. We hypothesize that maternal hyperglycemia alters the offspring pancreatic islet transcriptome, consequently conferring increased offspring susceptibility to developing pancreatic islet dysfunction. To create the fetal hyperglycemic environment, we employed a model capable of inducing localized fetal hyperglycemia in rats (Yao *et al.* 2010; Gordon *et al.* 2015). While maintaining maternal euglycemia, this model targets glucose delivery to fetuses residing in the left uterine horn, allowing the use of fetuses in the right uterine horn as genetically similar controls as they remain normoglycemic (Yao *et al.* 2010; Gordon *et al.* 2015). Using an RNA-sequencing approach, we identified early transcriptome alterations induced by late gestation hyperglycemia in fetal islets. Subsequently, we selected regenerating islet-derived protein 3-gamma (Reg3g) for validation due to its highest fold change and reported protective role as compensatory factor during islet stress (Marselli 2010, Xia 2016). Based on the biological processes enriched and functions of differentially expressed genes, we performed additional *ex-* and *in-vivo* studies evaluating weanling and offspring pancreatic islet cell viability and insulin secretory function. Together, our results showed that offspring exposed to late gestational hyperglycemia acute developed pancreatic islet morphological changes with altered

Accepted Manuscript published as JOE-18-0493.R1. Accepted for publication: 30-Nov-2018

105 islet transcriptomes that have critical functions on pancreatic islet health, and subsequently
106 developed persistent pancreatic islet dysfunction as early as weaning.
107
108 **METHODS**
109 **Animals:** All procedures conformed to the regulations of the Animal Welfare Act and the
110 National Institutes of Health Guide for the Care and Use of Laboratory Animals, and were
111 approved by the Indiana University School of Medicine Institutional Animal Care and Use
112 Committee. Rodents were housed in a temperature controlled, 12-hour light-dark cycled animal
113 care facility with free access to water and regular chow.
114
115 **Localized Fetomaternal Hyperglycemia (Figure 1A):** On gestation day (GD) 20, a vascular
116 catheter draining into the left uterine artery was placed in timed pregnant CD Sprague Dawley
117 rats (Charles River, Wilmington MA) to infuse glucose directly into the left uterine artery (Yao *et*
118 *al.* 2010; Gordon *et al.* 2015). Maternal tail vein blood glucose levels were measured prior to
119 anesthesia (n=13 GD 20 dams). Anesthesia was induced using isoflurane inhalation with
120 oxygen. A 3 Fr Polyurethane Catheter (Norfolk Access, IL) was inserted and secured 1.75 cm
121 retrograde into the femoral artery, thus placing the tip of the catheter several millimeters
122 proximal to uterine artery divergence from the common iliac artery. The left inferior peritoneal
123 space was explored and superfine microclips (GEM 1521, Synovis Micro Companies Alliance
124 Inc, AL) were placed on the superior gluteal and hypogastric trunk arteries. The catheter was
125 tunneled subcutaneously to exit at the mid-scapular space and connected to a single channel
126 infusion swivel (Instech, PA), allowing rats to move freely. Following this procedure, glucose
127 (D20W) was infused at 4 mg/min (20 µl/min) until GD22 (term). All pregnant dams received the
128 same postoperative analgesia. Topical Bupivacaine was applied immediately after wound
129 closure and subcutaneous buprenorphine SR (0.5 mg/kg) was given once preoperatively with
130 Meloxicam (3 mg/kg) once daily until delivery. After measuring maternal tail vein glucose level

(n=13 GD22 dams), GD 22 pregnant dams were anesthetized for laparotomy. Left and right uterine vein blood was collected prior to fetal extraction for glucose measurement using an Alphatrak Glucometer (Zoetis, NJ) (n=15 GD22 dams). After delivery, pups exposed to hyperglycemic infusion (HG) and respective right uterine horn controls (Con) were either euthanized for sample collection and blood glucose measurement (n 22-26 fetus; 12-14 neonates per group), or resuscitated and cross-fostered to healthy dams who delivered a day apart. Negative control experiment was performed using the same surgical approach but with dams were infused with normal saline (n=3 GD20 pregnant dams).

Islet Isolation: Fetal pups were euthanized immediately after delivery and the abdominal surface was sterilized with 70% ethanol. Laparotomy was performed and the fetal pancreas was separated from surrounding tissue starting from the spleen. One pancreas from each gender was pooled and cut into pieces smaller than 3 mm. Collagenase (Worthington, 1 ml of 2 mg/ml concentration per pancreas) was added and the tissue/collagenase mixture was incubated at 37°C for 10-12 minutes with intermittent manual shaking. Subsequently, a 10 ml syringe attached to 20 G needle was used for aspiration-ejection to homogenize the tissue lysates. Next HBSS/BSA was added to deactivate collagenase. The lysate was centrifuged, supernatant was removed, and the digested pellet was resuspended with RPMI 1640 media. Lastly, islets were hand-picked and cultured in RPMI 1640 media with 5.5 mM glucose. For weanlings, islets were isolated per standard ductal inflation technique (Stull *et al.* 2012).

RNA sequencing: The mRNA sequencing was performed by the Center for Medical Genomics at the Indiana University School of Medicine. Fetal islets were isolated as described above. Three set of paired fetal islet samples collected from fetuses from three independent infusions were used for RNA sequencing. Total islet RNA was extracted using an RNeasy micro kit (Qiagen, Valencia, CA) following the manufacturer's instructions. Purified total RNA was first

Accepted Manuscript published as JOE-18-0493.R1. Accepted for publication: 30-Nov-2018

157 evaluated for its quantity and quality using the Agilent Bioanalyzer 2100. A RIN (RNA Integrity
158 Number) of five or higher was required to pass the quality control. 65-150 ng of total RNA per
159 sample were used for library preparation. cDNA library was generated and indexed individually.
160 The cDNA library preparation included mRNA purification/enrichment, RNA fragmentation,
161 cDNA synthesis, ligation of index adaptors, and amplification following the TruSeq Stranded
162 mRNA Sample Preparation Guide (RS-122-9004DOC, Part# 15031047 Rev. E; Illumina, Inc.).
163 Each resulting indexed library was quantified and its quality assessed by Qubit and Agilent
164 Bioanalyzer, then pooled in equal molarity according to the Guide. Average size of library insert
165 was about 150b. Five microliters of 2 nM pooled libraries per lane were then denatured,
166 neutralized and applied to the cBot for flow cell deposition and cluster amplification, before
167 loading on to HiSeq 4000 for 75b paired-end sequencing (Illumina, Inc.). A Phred quality score
168 (Q score) was used to measure the quality of sequencing. More than 90% of the sequencing
169 reads reached Q30 (99.9% base call accuracy). Median raw reads were 41 million per sample.
170 The sequencing data were mapped to the rat genome (UCSC rn6) using a STAR RNA-seq
171 aligner (Dobin *et al.* 2013) and read counts were summarized using featureCounts (subread)
172 (Dobin *et al.* 2013; Liao *et al.* 2013) to get gene expression data. Seventy three percent of the
173 reads were mapped to the gene area. The genes with no/low expression were removed and the
174 expression data were normalized using the trimmed mean of M values (TMM) method.
175 Differential expression analysis was performed using edgeR (Robinson *et al.* 2009; McCarthy *et*
176 *al.* 2012), and the false discovery rate (FDR) was computed from p-values using the Benjamini-
177 Hochberg procedure (n= three paired replicates per group from three separate infusions).
178 Sequencing data can be found at GEO (GSE118323).
179
180 **Ingenuity Pathway Analysis (IPA) Package and GO Biological Process Enrichment:**
181 Differentially expressed genes (FDR<0.05 and FC>1.5) were analyzed using two pathway
182 analyses. IPA Package was used to identify enriched pathways and disease processes

(adjusted p-value <0.05 after Bonferroni correction). Next, the GO biological processes enriched by up- and down-regulated genes were identified separately using the PANTHER overrepresentation test (database version: GO Ontology database Released 2018-05-21, Reference List: Rattus Norvegicus, Annotation Data Set: GO Biological Process complete, Test Type: Fisher's Exact With FDR multiple test correction, FDR<0.05 as significant) (Mi *et al.* 2017) and visualized using REVIGO (Supek *et al.* 2011).

Quantitative RT-PCR (RT-qPCR): Additional sets of paired fetal islet samples collected as described above were used to validating RNA-sequencing findings (n= 5 paired replicates from five mothers, of those one was technical replicate from RNA-seq). For RT-qPCR, total RNA was purified and reverse transcribed at 37°C with 15 µg of random hexamers, 0.5 mM dNTPs, 5X first strand buffer, 0.01 mM dithiothreitol, and 200 U of M-MLV reverse transcriptase (Invitrogen) in a final reaction volume of 20 µl. RT-qPCR was performed using a SyBr Green-based methodology and primers that were synthesized commercially (Table 1). Briefly, 0.4 µl of forward primer (5 µM), 0.4 µL of reverse primer (5 µM), 5 µL of 2X SYBR Green PCR Master mix (applied Biosystems, NBY), and 4.2 µL of cDNA were mixed. Next, the reactions were amplified for 40 cycles using Applied Biosystems QuantStudio 3 Real-Time PCR system (Applied Biosystems CA).

Immunohistochemistry/Immunofluorescence: Pancreas was removed from animals after euthanasia and fixed rapidly, embedded in paraffin, and sectioned into 5 µm thick slices, with one section of each group on the same slide to avoid slide-to-slide variation. Two to three sections per animal were analyzed for all immunohistochemistry/immunofluorescence studies. The pancreatic sections were deparaffinized and rehydrated through a series of graded ethanol solutions. Endogenous peroxidase activity blockade was performed and antigens were retrieved by microwaving slides with unmasking solution (Vector Laboratories, CA). To identify pancreatic

Accepted Manuscript published as JOE-18-0493.R1. Accepted for publication: 30-Nov-2018

endocrine cell areas (Fetus: 5-6 pups/group from five mothers; adult offspring: 4 males/group from four mothers), sections were incubated with anti-insulin (Santa Cruz sc-9168, 1:500) or anti-glucagon antibodies (Santa Cruz sc-13091, 1:500) overnight. Digital images depicting whole pancreatic tissue sections were obtained using an Axio-Scan Z1 inverted microscope (Zeiss, Germany). The area of insulin- or glucagon-positive cells (calculated using Zen Pro) was divided by the total area of whole pancreatic sections to obtain the beta or alpha cell cross-sectional area as a percentage of total pancreatic area. For adult offspring, beta cell mass is calculated by multiplying percent insulin positive area with total pancreatic mass. To assess relative Reg3g distribution in beta cells (GD22 fetus: 5 pups/group from five mothers), we quantified the ratio of Reg3g-stained volume to that of insulin. Pancreatic sections were incubated with anti-insulin antibody (Santa Cruz sc-9168, 1:500) and anti-Reg3g antibody (Antibodies Online, ABIN3023039, 1:200) overnight. Pancreatic histological samples were scanned bidirectionally with a Leica TCS SP8 laser-scanning confocal microscope system equipped with a 405 nm diode laser and 488 nm and 552 nm semiconductor lasers and an HC PL APO CS2 40X/1.30 oil objective lens through a 68.06 µm pinhole (1.0 Airy unit). Emission bandwidths were set to 415-480 nm for blue emission, 495-545 nm for green emission, and 560-700 nm for red emission. Twelve-bit 1024x1024 voxel images were collected at a voxel volume of 0.212 µm x 0.212 µm x 0.502 µm with a line average setting of two using LAS X v3.1.5.16308 software. These settings were applied to all acquired images. All image processing was performed with Fiji version 1.51 (Schindelin *et al.* 2012). First, Reg3g and insulin images were thresholded with the Li algorithm in Fiji and a region of interest (ROI) was drawn around insulin-stained cells. All signal outside the ROI was removed and the insulin signal volume (μm^3) contained within the ROI was quantified with the 3D object counting function in Fiji. This ROI outline was transferred to the corresponding Reg3g image and all outside signal was removed. Subsequently, the signal volume (μm^3) within the insulin-defined ROI that was stained positively for Reg3g was measured. Finally, the relative expression of

Reg3g in beta cells was determined by calculating the ratio of Reg3g signal volume to insulin volume.

***Ex-vivo* Islet Glucose Stimulated Insulin Secretion (GSIS):** Isolated islets from weanlings (n=5 male weanlings/group from five mothers) were recovered in RPMI overnight prior to measuring insulin secretion under static glucose incubation (Komatsu *et al.* 1995; Mehta *et al.* 2016). 20-25 size-matched weanling islets were incubated in Krebs-Ringer bicarbonate buffer (129 mM NaCl, 5 mM $NaHCO_3$, 4.8 mM KCl, 1.2 mM KH_2PO_4, 2.5 mM $CaCl_2$, 1.2 mM $MgSO_4$, 0.1% BSA, 10 mM Hepes, pH 7.4) containing 2.8 mM glucose for 1 hour at 37°C (pre-incubation). Next, the incubation medium was removed by aspiration and 1 ml of fresh KRB buffer containing different concentrations of glucose was added (5.5 mM and 16.7 mM) to determine islet insulin secretory function at different glucose levels. At the end of incubations, the medium was aspirated and stored at -80°C until measurement. At the end of the static culture, total insulin of pancreatic islets was extracted using acid-ethanol extraction (1.5% HCl, 75% EtOH, 0.1% Triton). Weanling *ex-vivo* islet GSIS media insulin concentration was measured using Stellux Chemi Rodent Insulin Elisa (ALPCO, NH). Results were analyzed and presented as a percentage of total insulin.

***In-vivo* metabolic evaluations of offspring:** Metabolic phenotypes of weanlings and adult offspring were evaluated using intraperitoneal glucose tolerance testing (GTT) (weanling: total 14-19 males/group from 9 mothers; 2 month old adult: 6-7 males/group from 5 mothers) and intraperitoneal insulin tolerance testing (ITT) (n=4-6 male weanlings/group from 3 mothers). Animals were fasted for 6 hours prior to both tests. For GTT, 1 or 2 g/kg of glucose was injected intraperitoneally and blood was collected from animals via tail vein at 0, 10, 20, 30, 60, 90 and 120-minute time points. Additional blood was collected at 10 and 30 minutes from adult offspring for serum insulin measurement. For ITT, 0.75 U/kg of Humulin R (Eli Lilly, IN) was administered

Accepted Manuscript published as JOE-18-0493.R1. Accepted for publication: 30-Nov-2018

and blood glucose was measured at 0, 15, 30, 45, and 60-minute time points. Animal blood glucose levels were measured with an Alphatrak Glucometer (Zoetis, NJ). Fetal serum insulin concentrations were measured using the Ultrasensitive Rat Insulin ELISA kit (#90060, Crystal Chem, Downers Grove, IL). Adult serum insulin levels were measured using Stellux Chemi Rodent Insulin Elisa (ALPCO, NH).

Alamar blue cell viability assay: Isolated islets from weanlings (n=4 pups/group from 4 mothers) were recovered in RPMI 1640 media containing 11 mM glucose for 24 hours prior to evaluation. Seven to eight size-matched islets were handpicked into 96 well with 100 µl of regular RPMI media. Sterile alamar blue was subsequently added in 1:10 dilution and then read hourly with a FlexStation 3 Multi-Mode microplate reader (Molecular Devices, San Jose, Ca) at an excitation wavelength of 535 nm and emission wavelength of 585 nm. Between reads, islets were incubated in a humidified, warm tissue culture chamber. The fluorescence value produced by Con/HG wells was obtained by subtracting the relative fluorescence unit (RFU) of the negative control well (media and Alamar blue, no islets) from the measured RFU in each well at different timepoints.

Statistics: Each group of fetuses and male offspring originating from one biological mother was considered as n=1. In instances where more than one pups from the same mother were analyzed, the average of the acquired data would then be used as a single data (Vieleisis & Oh 1983; Roest *et al.* 2004; Gordon *et al.* 2015). All results were represented as mean ± SEM, while fold changes of RT-qPCR results were represented as log2FC in comparison to RNA-seq results. For single time-point measurement, the difference between two groups was assessed using a paired two-tailed t-test. For repeated measures (glucose level during GTT, ITT, GSIS, Alamar blue cell viability assay), two-way ANOVA tests followed by Bonferroni multiple

comparison tests correction were performed to assess the difference between two groups. Results were defined as statistically different when $p<0.05$.

RESULTS

Localized Fetomaternal Hyperglycemia Induces Fetal Pancreatic Islet Perturbations. The localized fetomaternal hyperglycemia model allows for dosage and temporal control over glucose delivery to left uterine horn fetuses (Fig 1A). To determine the effects of late gestation hyperglycemia, glucose was infused from GD20 to GD22, with offspring evaluated at different timepoints (Fig 1B). On GD22, maternal blood glucose concentrations were unchanged with ongoing 4 mg/min glucose infusion (Fig 1C). To validate the specific targeting of glucose delivery, we measured both the maternal uterine vein and fetal blood glucose level. Indeed, blood glucose concentrations from the maternal left uterine vein were higher than those from the right (Fig 1C). Compared to internal control fetuses from the right uterine horn (Con), left uterine horn fetal rats (HG) also had higher blood glucose levels (Fig 1D). As with previously published report (Gain *et al.* 1981), blood glucose levels of control pups were higher 30 minutes after birth (Fig 1D). In contrast, this increase in glucose level was not apparent in HG pups (Fig 1D). In fact, when compared to control, newborn pups that received glucose infusion had lower blood glucose levels (Fig 1D). Not surprisingly, left uterine pups exposed to glucose infusion also had higher serum insulin levels (Fig 1E) and beta cell areas (Fig 1F). The higher number of cells within insulin positive area in hyperglycemic pups (Supp Figure 1) indicating that the increase in beta cell area likely resulted from cellular hyperplasia. Taken together, fetal pups exposed to transient (48 hours) hyperglycemia developed both hyperinsulinemia and pancreatic beta cell hyperplasia.

RNA-seq identified differentially expressed genes known to mediate inflammation and pancreatic islet function. To identify the earliest pathway and biological processes altered by

Accepted Manuscript published as JOE-18-0493.R1. Accepted for publication: 30-Nov-2018

hyperglycemia exposure, we performed RNA-sequencing to examine whole islets transcriptome changes in GD22 fetal islets immediately after completing 48 hours of glucose infusion. Compared to controls, HG fetal islets had 87 differentially expressed genes (DEGs) (69 up- and 18 down-regulated) (Supp Table 1). The result of Ingenuity Pathway Analysis revealed 22 enriched pathways, the majority of which were related to inflammation (Supp Table 2). IPA also identified diabetes mellitus as a relevant disease process (24 DEGs) and also predicted the activation of cell death (41 DEGs) (Fig 2A). Next, the biological processes enriched by up- and down-regulated genes were identified using the PANTHER classification system (Mi *et al.* 2017) and visualized using REVIGO (Supek *et al.* 2011). As shown in the semantic similarity-based scatterplots, the up- and down-regulated genes were involved in different biological processes (Fig 2B). While the up-regulated DEGs were heavily enriched in inflammatory and immune system related biological processes, the down-regulated genes were involved in more diverse biological processes (Fig 2B). In addition to inflammation, the down-regulated genes were also enriched in processes involving cellular responses to stimuli and developmental processes (table in Fig 2B). To further understand the specific biological implications of these broad terms, we performed a literature review and identified a significant number of down-regulated genes (*Ctgf, Clu, Cftr, Fgfr3, Gabrp, Mmp7, Reg3b, Reg3g*) that are involved in early pancreatic islet development (proliferation, new islet formation) (Crawford *et al.* 2009; Koivula *et al.* 2016), adult pancreatic islet function, neogenesis, and anti-apoptotic effects during stress (Table 2). Further RT-qPCR validation confirmed both *Reg3g* and *Reg3b*, along with two additional down-regulated genes (*Gabrp* and *Mmp7*), were consistently decreased in GD22 islets exposed to *in-utero* hyperglycemia (Fig 3A). Furthermore, HG pups revealed a decrease in the percentage of area positive for REG3G staining within insulin-positive cells (Fig 3B), indicating that HG beta cells had diminished REG3G protein expression. Collectively, RNA-sequencing results revealed that fetal hyperglycemia induces the islet transcriptome associated with diabetes mellitus and

activated islet inflammation/cell death pathways. Interestingly, the down-regulated genes are involved in various biological processes that modulate pancreatic islet health.

Pancreatic islet dysfunction occurs in weanlings exposed to hyperglycemia *in-utero.* Given that late gestational hyperglycemia rapidly alters fetal pancreatic islet phenotypes and transcriptome, it was thus of interest to determine whether offspring were vulnerable to developing pancreatic islet dysfunction. Particularly, we aimed to determine if late gestation hyperglycemia exposure altered offspring pancreatic islet viability and function as predicted by transcriptome analysis. At weaning (P21), HG pups developed impaired glucose tolerance as evidenced by higher glucose levels at 10 min during IPGTT and higher incremental AUC (iAUC) (Fig 4A-D). Using the same surgical approach, we performed a separate negative control experiment by infusing normal saline to left uterine horn fetal pups. We observed no difference in IPGTT of saline-infused offspring from the left uterine horn when compared to their internal controls from the right uterine horn (Supp Figure 2). Next, we evaluated weanling pancreatic islet cell viability using the Alamar blue cell viability assay (Muthyala *et al.* 2017) and insulin secretory function via *ex-vivo* static GSIS. Under basal conditions, pancreatic islets extracted from HG weanlings had lower cell viability suggesting an increased susceptibility to cell death (Fig 4E). Additionally, HG weanling islets had decreased insulin secretion at both 5.6 mM and 16.7 mM stimulatory phases (Fig 4F). In the absence of overt insulin resistance during insulin tolerance testing (Fig 4I), these findings assert that offspring exposed to late gestation hyperglycemia developed glucose intolerance secondary to pancreatic islet dysfunction as observed by decreased cell viability and static glucose-stimulated insulin release.

Adult offspring exposed to HG had decreased beta cell mass and insulin secretory dysfunction without altered growth or increased inflammatory mediators. We sought to determine if pancreatic islet changes at weaning would impact adult offspring. As beta cell mass

Accepted Manuscript published as JOE-18-0493.R1. Accepted for publication: 30-Nov-2018

and function increase drastically after weaning (Bonner-Weir *et al.* 2016), we hypothesized that increased susceptibility to cell death and decreased glucose responsiveness in weanling islets would impact both pancreatic beta cell mass and insulin secretory function in HG adults. Indeed, HG adult offspring remained glucose intolerant with an increased glucose tolerance curve divergence (Fig 5A, B). Despite a higher serum glucose level, HG adults had diminished *in-vivo* insulin release 10 minutes after glucose injection (Fig 5C). Additionally, HG adults also had lower pancreatic beta cell mass (Fig 5D-F). To determine if altered growth or increased adiposity contributed to glucose intolerance, we measured offspring weight and adiposity at weaning and at two months old. There were no differences between offspring who received *in-utero* hyperglycemic infusion and their respective controls (Fig 5G, H). Since the inflammatory pathways were overrepresented, we also measured five inflammasomes in fetal, neonatal and two month old offspring, in which three were IPA-predicted (IFNG, TNF-alpha, IL1B) and two were associated with the up-regulated DEGs (CXCL10, IL-17). However, the levels of these inflammatory mediators in the serum both during early life and at two months old were unchanged (Supp Figure 3). These findings indicated that pancreatic islet dysfunction was not mediated by altered growth, increased adiposity, or systemic inflammation.

DISCUSSION

Independent of genetic risk, offspring born from diabetic pregnancies experience a greater risk of insulin resistance, pancreatic islet dysfunction, and type 2 diabetes (Ratner *et al.* 2008; Fraser & Lawlor 2014; Tam *et al.* 2017; Das Gupta *et al.* 2018). Such risk of transmission is thought to result from maternal hyperglycemia (Kubo *et al.* 2014; Tam *et al.* 2017; Kawasaki *et al.* 2018); however, no direct evidence exists elucidating the exact role of maternal hyperglycemia in programming offspring metabolic health. Our fetomaternal hyperglycemia model, capable of inducing localized maternal and fetal hyperglycemia, addresses this knowledge gap. Using this model, where late gestation fetal pups were exposed to mild-

moderate hyperglycemia (<350mg/dL) (Aerts & van Assche 1977; Blondeau *et al.* 2011; White *et al.* 2015), we first showed that hyperglycemic rodent offspring acutely developed a pancreatic islet phenotype similar to that of an infant of a diabetic mother(Helwig 1940; Cardell 1953) and identified DEGs that modulate pancreatic islet inflammation, cell viability, and function. Along with transcriptome changes, metabolic testing during weaning showed that offspring exposed to hyperglycemia *in-utero* developed glucose intolerance due to increased pancreatic islet susceptibility to cell death and decreased glucose-induced insulin secretion. Finally, consistent with the altered fetal islet transcriptome and findings in weanlings, adult offspring exposed to late gestation hyperglycemia showed decreased beta cell mass and insulin secretory function.

There are a number of investigations that performed targeted molecular studies on offspring exposed to different diabetic pregnancy models. These studies identified that pancreatic islets collected from young offspring exposed to diabetic milieu *in-utero* had altered IGF2/insulin receptor signaling (Ding *et al.* 2012; Bringhenti *et al.* 2016), altered glucose metabolism (Han *et al.* 2007; Cerf *et al.* 2009), and/or increased oxidative stress/inflammation (Wang *et al.* 2014; Yokomizo *et al.* 2014). While the hyperglycemic islet transcriptome predicted heightened inflammation, the DEGs and pathway analysis did not show changes in genes related to IGF2/insulin receptor signaling or enzymes regulating pancreatic islet glucose metabolism. This discrepancy could be due to multiple reasons, the first being the difference in our model and timepoint examination of offspring islets. Our model addressed the direct effects of hyperglycemia during late gestation, as opposed to other models that exposed the fetus to more complex metabolic perturbations throughout pregnancy and subsequently addressing the molecular pathways altered in offspring later in life. Additionally, all of the aforementioned studies, except for Ding *et al.* (2012), examined the effects of maternal diabetes/overnutrition in young adult offspring.

Accepted Manuscript published as JOE-18-0493.R1. Accepted for publication: 30-Nov-2018

Overall, the transcriptome analysis and literature review on individual DEGs predicted three major processes that regulate offspring pancreatic islet health: increased inflammation, susceptibility to cell death, and decreased pancreatic islet insulin secretion. Particularly, the up-regulated genes were heavily enriched in inflammatory pathways and an activated cell death process. Since there was absence of systemic inflammation, we reasoned that increased inflammation is not the primary mechanism inducing offspring pancreatic islet dysfunction. Rather, we hypothesized that the observed increased in inflammatory-related transcriptome in offspring exposed to late gestation hyperglycemia is stimulated by the increased in pancreatic islet susceptibility to cell death. The down-regulated genes are closely related to pancreatic islet cells (Supp Table 3) and appear to have more diverse biological roles ranging from modulating pancreatic islet development, inflammatory response, anti-apoptotic effects, and normal/compensatory beta cell insulin secretion (table 2). The cystic fibrosis transmembrane conductance regulator (*Cftr*) has been increasingly recognized for its importance in cystic fibrosis-related diabetes (CFRD): the pathogenesis of which involves altered early life pancreatic islet morphogenesis (Rotti *et al.* 2018) and beta cell loss and intra-islet inflammation (Hart *et al.* 2018). Connective tissue growth factor (*Ctgf*) and fibroblast growth factor receptor 3 (*Fgfr3*) are another two down-regulated genes that can affect early postnatal pancreatic islet development both morphologically and functionally. Both of these genes are expressed only in late embryonic beta cell development and emerging islets (Arnaud-Dabernat *et al.* 2007; Crawford *et al.* 2009). Particularly, *Ctgf* inactivation during embryogenesis caused decreased insulin positive cells (Crawford *et al.* 2009), while *Ctgf* haplo-insufficiency mice had decreased beta cell proliferation during pregnancy (Pasek *et al.* 2017).

Interestingly, the two most down-regulated genes, *Reg3g* and *Reg3b,* were from the common Regenerating Islet-Derived Protein (REG protein) family. Based on DNA sequence and protein structure similarities, these two REG proteins are classified under Type 3 REG (Abe *et*

441 *al.* 2000), which is expressed in pancreatic tissue (Parikh *et al.* 2012) and suggested to pattern
442 embryonic endocrine cells (Hamblet *et al.* 2008). REG gene expression levels correlate with
443 insulin secretory function (Madrid *et al.* 2013) and treatment using INGAP, one of the subtypes
444 of REG protein, enhances neonatal islet insulin secretion (Barbosa *et al.* 2006; Madrid *et al.*
445 2009). More importantly, REG protein expression is up-regulated in diabetic human islets
446 (Marselli *et al.* 2010; Planas *et al.* 2010), with animal models supporting their role as a
447 compensatory factor during islet stress (Siddique & Awan 2016; Xia *et al.* 2016). In regard to the
448 downstream signaling pathway, *ex-vivo* (keratinocytes) (Barbosa *et al.* 2008; Lai *et al.* 2012; Wu
449 *et al.* 2016) and *in-vivo* (Xia *et al.* 2016) studies have indicated that REG3G/REG3A protein
450 binds to Extl3, which subsequently activates AKT and/or STAT3 downstream signaling. While
451 we have not performed further protein evaluation in our model, IPA indicated the involvement of
452 STAT3 pathway (-log p-value = 3.28) with STAT3 predicted as an inhibited upstream regulator
453 with the lowest Z-score (Exp FC:-1.214, Z-score = -3.65, -log p-value = 16.8, -log adjusted p-
454 value = 14.0). Considering these reported roles of REG protein, our findings indicate that
455 decreased *Reg3g* and/or *Reg3b* in pups exposed to hyperglycemia *in-utero* would negatively
456 impact postnatal pancreatic islet formation and/or functional maturation leading to decreased
457 offspring islet cell viability and function. Therefore, future studies are warranted to determine the
458 implication of decreased Type 3 REG during early postnatal pancreatic islet development (Lai *et*
459 *al.* 2012; Wu *et al.* 2016).
460
461 Both pancreatic beta cell mass and glucose responsiveness increase most significantly
462 after weaning (Jacovetti *et al.* 2015; Bonner-Weir *et al.* 2016); changes in islet susceptibility to
463 cell death and decrease in function could determine pancreatic islet mass and function in
464 adulthood. Therefore, it is not surprising that the findings describing increased susceptibility to
465 cell death and the insulin secretory defect during weaning negatively impacted HG offspring
466 pancreatic beta cell mass and insulin secretory defect. This finding is consistent with both

 Accepted Manuscript published as JOE-18-0493.R1. Accepted for publication: 30-Nov-2018

human epidemiological data (Tam *et al.* 2017) and an animal model mimicking diabetic pregnancy with mild-to-moderate maternal hyperglycemia (<350mg/dL) (Aerts & van Assche 1977; Blondeau *et al.* 2011; White *et al.* 2015). Most importantly, we showed that late gestation hyperglycemia, even for a short duration (<10% of pregnancy), exhibited long-lasting negative impacts on offspring pancreatic islet function. These findings stress not only the critical role of maternal hyperglycemia, but also the importance of examining the metabolic outcome of offspring early in life for both human and animal studies.

Conclusion

In conclusion, late gestation hyperglycemia perturbs fetal pancreatic islet morphology and diminishes insulin secretory function in young offspring. Transcriptome analysis indicated that GD22 islets exposed to *in-utero* hyperglycemia displayed heightened inflammatory responses, increased susceptibility to cell death and decreased pancreatic islet insulin secretory function. This finding guided our study to identify pancreatic islet dysfunction in weanlings, which predisposed adult offspring to decreased beta cell mass and insulin secretion. Our transcriptome analysis provides a paradigm for elucidating the programming mechanism resulting from excessive glucose exposure. Future studies validating the targets in modulating postnatal pancreatic islet neogenesis and function are warranted.

Declaration of Interest

The authors declare that there is no conflict of interest that could be perceived as prejudicing the impartiality of the study.

Funding

This project was funded by the Riley Children's Foundation Physician Scientists Scholar Award (KLK).

493

494 **Author contribution statement**

495 Conceived study: KLK, JC, YJ. Designed and performed experiments: KLK, JC, YJ, XX. Data
496 analysis: KLK, XR (RNA-seq), MEB (Immunofluorescence & image analysis). Results
497 interpretation: All authors. Manuscript preparation: JC, YJ, MEB, KLK. All authors reviewed and
498 approved of the manuscript.

499

500 **Acknowledgement:**

501 We thank Dr Carmella Evans-Molina, Dr Paul Rozance, Dr Laura Haneline, Dr Christina
502 Santangelo (I3 Program), and Dr John Paul Spence (I3 Program) for reviewing the manuscript.
503 We also thank Jun Wang and Jun Li from the Center of Medical Genomics at Indiana University
504 School of Medicine for performing RNA sequencing.

Accepted Manuscript published as JOE-18-0493.R1. Accepted for publication: 30-Nov-2018

References

Abe M, Nata K, Akiyama T, Shervani NJ, Kobayashi S, Tomioka-Kumagai T, Ito S, Takasawa S & Okamoto H 2000 Identification of a novel Reg family gene, Reg IIIδ, and mapping of all three types of Reg family gene in a 75 kilobase mouse genomic region. *Gene* **246** 111–122.

Aerts L & van Assche FA 1977 Rat foetal endocrine pancreas in experimental diabetes. *The Journal of Endocrinology* **73** 339–346.

Arnaud-Dabernat S, Kritzik M, Kayali AG, Zhang Y-Q, Liu G, Ungles C & Sarvetnick N 2007 FGFR3 is a negative regulator of the expansion of pancreatic epithelial cells. *Diabetes* **56** 96–106.

Artner I, Blanchi B, Raum JC, Guo M, Kaneko T, Cordes S, Sieweke M & Stein R 2007 MafB is required for islet beta cell maturation. *Proceedings of the National Academy of Sciences of the United States of America* **104** 3853–3858.

Barbosa H, Bordin S, Stoppiglia L, Silva K, Borelli M, Del Zotto H, Gagliardino J & Boschero A 2006 Islet Neogenesis Associated Protein (INGAP) modulates gene expression in cultured neonatal rat islets. *Regulatory Peptides* **136** 78–84.

Barbosa HC, Bordin S, Anhê G, Persaud SJ, Bowe J, Borelli MI, Gagliardino JJ & Boschero AC 2008 Islet neogenesis-associated protein signaling in neonatal pancreatic rat islets: involvement of the cholinergic pathway. *The Journal of Endocrinology* **199** 299–306.

Blondeau B, Joly B, Perret C, Prince S, Bruneval P, Lelièvre-Pégorier M, Fassot C & Duong Van Huyen J-P 2011 Exposure in utero to maternal diabetes leads to glucose intolerance and high blood pressure with no major effects on lipid metabolism. *Diabetes & Metabolism* **37** 245–251.

Bonner-Weir S, Aguayo-Mazzucato C & Weir GC 2016 Dynamic development of the pancreas from birth to adulthood. *Upsala Journal of Medical Sciences* **121** 155–158.

Bringhenti I, Ornellas F, Mandarim-de-Lacerda CA & Aguila MB 2016 The insulin-signaling pathway of the pancreatic islet is impaired in adult mice offspring of mothers fed a high-fat diet. *Nutrition* **32** 1138–1143.

Cardell BS 1953 The infants of diabetic mothers; a morphological study. *The Journal of Obstetrics and Gynaecology of the British Empire* **60** 834–853.

Cerf ME, Muller CJ, Du Toit DF, Louw J & Wolfe-Coote SA 2006 Hyperglycaemia and reduced glucokinase expression in weanling offspring from dams maintained on a high-fat diet. *The British Journal of Nutrition* **95** 391–396.

Cerf ME, Chapman CS, Muller CJ & Louw J 2009 Gestational high-fat programming impairs insulin release and reduces Pdx-1 and glucokinase immunoreactivity in neonatal Wistar rats. *Metabolism: Clinical and Experimental* **58** 1787–1792.

Clausen TD, Mathiesen ER, Hansen T, Pedersen O, Jensen DM, Lauenborg J & Damm P 2008 High prevalence of type 2 diabetes and pre-diabetes in adult offspring of women with

gestational diabetes mellitus or type 1 diabetes: the role of intrauterine hyperglycemia. *Diabetes Care* **31** 340–346.

Crawford LA, Guney MA, Oh YA, Andrea DeYoung R, Valenzuela DM, Murphy AJ, Yancopoulos GD, Lyons KM, Brigstock DR, Economides A *et al.* 2009 Connective Tissue Growth Factor (CTGF) Inactivation Leads to Defects in Islet Cell Lineage Allocation and β-Cell Proliferation during Embryogenesis. *Molecular Endocrinology* **23** 324–336.

Das Gupta R, Gupta S, Das A, Biswas T, Haider MR & Sarker M 2018 Ethnic predisposition of diabetes mellitus in the patients with previous history of gestational diabetes mellitus: a review. *Expert Review of Endocrinology & Metabolism* **13** 149–158.

DeSisto CL 2014 Prevalence Estimates of Gestational Diabetes Mellitus in the United States, Pregnancy Risk Assessment Monitoring System (PRAMS), 2007–2010. *Preventing Chronic Disease* **11**. (doi:10.5888/pcd11.130415)

Ding G-L, Wang F-F, Shu J, Tian S, Jiang Y, Zhang D, Wang N, Luo Q, Zhang Y, Jin F *et al.* 2012 Transgenerational glucose intolerance with Igf2/H19 epigenetic alterations in mouse islet induced by intrauterine hyperglycemia. *Diabetes* **61** 1133–1142.

Dobin A, Davis CA, Schlesinger F, Drenkow J, Zaleski C, Jha S, Batut P, Chaisson M & Gingeras TR 2013 STAR: ultrafast universal RNA-seq aligner. *Bioinformatics* **29** 15–21.

Fraser A & Lawlor DA 2014 Long-term health outcomes in offspring born to women with diabetes in pregnancy. *Current Diabetes Reports* **14** 489.

Frost MS, Zehri AH, Limesand SW, Hay WW Jr & Rozance PJ 2012 Differential effects of chronic pulsatile versus chronic constant maternal hyperglycemia on fetal pancreatic β-cells. *Journal of Pregnancy* **2012** 812094.

Gain KR, Malthus R & Watts C 1981 Glucose homeostasis during the perinatal period in normal rats and rats with a glycogen storage disorder. *The Journal of Clinical Investigation* **67** 1569–1573.

Gautier JF, Wilson C, Weyer C, Mott D, Knowler WC, Cavaghan M, Polonsky KS, Bogardus C & Pratley RE 2001 Low acute insulin secretory responses in adult offspring of people with early onset type 2 diabetes. *Diabetes* **50** 1828–1833.

Gordon EE, Reinking BE, Hu S, Yao J, Kua KL, Younes AK, Wang C, Segar JL & Norris AW 2015 Maternal Hyperglycemia Directly and Rapidly Induces Cardiac Septal Overgrowth in Fetal Rats. *Journal of Diabetes Research* **2015** 479565.

Green AS, Chen X, Macko AR, Anderson MJ, Kelly AC, Hart NJ, Lynch RM & Limesand SW 2012 Chronic pulsatile hyperglycemia reduces insulin secretion and increases accumulation of reactive oxygen species in fetal sheep islets. *The Journal of Endocrinology* **212** 327–342.

Hamblet NS, Shi W, Vinik AI & Taylor-Fishwick DA 2008 The Reg family member INGAP is a marker of endocrine patterning in the embryonic pancreas. *Pancreas* **36** 1–9.

Han J, Xu J, Long YS, Epstein PN & Liu YQ 2007 Rat maternal diabetes impairs pancreatic beta-cell function in the offspring. *American Journal of Physiology. Endocrinology and*

Accepted Manuscript published as JOE-18-0493.R1. Accepted for publication: 30-Nov-2018

Metabolism **293** E228–E236.

Hart NJ, Aramandla R, Poffenberger G, Fayolle C, Thames AH, Bautista A, Spigelman AF, Babon JAB, DeNicola ME, Dadi PK *et al.* 2018 Cystic fibrosis-related diabetes is caused by islet loss and inflammation. *JCI Insight* **3**. (doi:10.1172/jci.insight.98240)

Helwig EB 1940 HYPERTROPHY AND HYPERPLASIA OF ISLANDS OF LANGERHANS IN INFANTS BORN OF DIABETIC MOTHERS. *Archives of Internal Medicine* **65** 221.

Hunt KJ & Schuller KL 2007 The increasing prevalence of diabetes in pregnancy. *Obstetrics and Gynecology Clinics of North America* **34** 173–199, vii.

Jacovetti C, Matkovich SJ, Rodriguez-Trejo A, Guay C & Regazzi R 2015 Postnatal β-cell maturation is associated with islet-specific microRNA changes induced by nutrient shifts at weaning. *Nature Communications* **6** 8084.

Jacovetti C, Rodriguez-Trejo A, Guay C, Sobel J, Gattesco S, Petrenko V, Saini C, Dibner C & Regazzi R 2017 MicroRNAs modulate core-clock gene expression in pancreatic islets during early postnatal life in rats. *Diabetologia* **60** 2011–2020.

Kawasaki M, Arata N, Miyazaki C, Mori R, Kikuchi T, Ogawa Y & Ota E 2018 Obesity and abnormal glucose tolerance in offspring of diabetic mothers: A systematic review and meta-analysis. *PloS One* **13** e0190676.

Koivula FNM, McClenaghan NH, Harper AGS & Kelly C 2016 Islet-intrinsic effects of CFTR mutation. *Diabetologia* **59** 1350–1355.

Komatsu M, Schermerhorn T, Aizawa T & Sharp GW 1995 Glucose stimulation of insulin release in the absence of extracellular Ca2 and in the absence of any increase in intracellular Ca2 in rat pancreatic islets. *Proceedings of the National Academy of Sciences* **92** 10728–10732.

Kubo A, Ferrara A, Windham GC, Greenspan LC, Deardorff J, Hiatt RA, Quesenberry CP Jr, Laurent C, Mirabedi AS & Kushi LH 2014 Maternal hyperglycemia during pregnancy predicts adiposity of the offspring. *Diabetes Care* **37** 2996–3002.

Lai Y, Li D, Li C, Muehleisen B, Radek KA, Park HJ, Jiang Z, Li Z, Lei H, Quan Y *et al.* 2012 The antimicrobial protein REG3A regulates keratinocyte proliferation and differentiation after skin injury. *Immunity* **37** 74–84.

Liao Y, Smyth GK & Shi W 2013 featureCounts: an efficient general purpose program for assigning sequence reads to genomic features. *Bioinformatics* **30** 923–930.

Madrid V, Del Zotto H, Maiztegui B, Raschia MA, Alzugaray ME, Boschero AC, Barbosa HC, Flores LE, Borelli MI & Gagliardino JJ 2009 Islet neogenesis-associated protein pentadecapeptide (INGAP-PP): mechanisms involved in its effect upon beta-cell mass and function. *Regulatory Peptides* **157** 25–31.

Madrid V, Borelli MI, Maiztegui B, Flores LE, Gagliardino JJ & Zotto HD 2013 Islet neogenesis-associated protein (INGAP)-positive cell mass, β-cell mass, and insulin secretion: their relationship during the fetal and neonatal periods. *Pancreas* **42** 422–428.

Marselli L, Thorne J, Dahiya S, Sgroi DC, Sharma A, Bonner-Weir S, Marchetti P & Weir GC

2010 Gene expression profiles of Beta-cell enriched tissue obtained by laser capture microdissection from subjects with type 2 diabetes. *PloS One* **5** e11499.

Martin B & Sacks DA 2018 The global burden of hyperglycemia in pregnancy - Trends from studies in the last decade. *Diabetes Research and Clinical Practice*. (doi:10.1016/j.diabres.2018.04.003)

McCarthy DJ, Chen Y & Smyth GK 2012 Differential expression analysis of multifactor RNA-Seq experiments with respect to biological variation. *Nucleic Acids Research* **40** 4288–4297.

Mehta ZB, Fine N, Pullen TJ, Cane MC, Hu M, Chabosseau P, Meur G, Velayos-Baeza A, Monaco AP, Marselli L *et al.* 2016 Changes in the expression of the type 2 diabetes-associated gene VPS13C in the β-cell are associated with glucose intolerance in humans and mice. *American Journal of Physiology. Endocrinology and Metabolism* **311** E488–E507.

van der Meulen T & Huising MO 2014 Maturation of stem cell-derived beta-cells guided by the expression of urocortin 3. *The Review of Diabetic Studies: RDS* **11** 115–132.

Mi H, Huang X, Muruganujan A, Tang H, Mills C, Kang D & Thomas PD 2017 PANTHER version 11: expanded annotation data from Gene Ontology and Reactome pathways, and data analysis tool enhancements. *Nucleic Acids Research* **45** D183–D189.

Muthyala S, Safley S, Gordan K, Barber G, Weber C & Sambanis A 2017 The effect of hypoxia on free and encapsulated adult porcine islets-an in vitro study. *Xenotransplantation* **24**. (doi:10.1111/xen.12275)

Parikh A, Stephan A-F & Tzanakakis ES 2012 Regenerating proteins and their expression, regulation and signaling. *Biomolecular Concepts* **3** 57–70.

Pasek RC, Dunn JC, Elsakr JM, Aramandla M, Matta AR & Gannon M 2017 Vascular-derived connective tissue growth factor (Ctgf) is critical for pregnancy-induced β cell hyperplasia in adult mice. *Islets* **9** 150–158.

Planas R, Carrillo J, Sanchez A, de Villa MCR, Nuñez F, Verdaguer J, James RFL, Pujol-Borrell R & Vives-Pi M 2010 Gene expression profiles for the human pancreas and purified islets in type 1 diabetes: new findings at clinical onset and in long-standing diabetes. *Clinical and Experimental Immunology* **159** 23–44.

Raghavan S, Zhang W, Yang IV, Lange LA, Lange EM, Fingerlin TE & Dabelea D 2017 Association between gestational diabetes mellitus exposure and childhood adiposity is not substantially explained by offspring genetic risk of obesity. *Diabetic Medicine: A Journal of the British Diabetic Association* **34** 1696–1700.

Ratner RE, Christophi CA, Metzger BE, Dabelea D, Bennett PH, Pi-Sunyer X, Fowler S, Kahn SE & Diabetes Prevention Program Research Group 2008 Prevention of diabetes in women with a history of gestational diabetes: effects of metformin and lifestyle interventions. *The Journal of Clinical Endocrinology and Metabolism* **93** 4774–4779.

Robinson MD, McCarthy DJ & Smyth GK 2009 edgeR: a Bioconductor package for differential expression analysis of digital gene expression data. *Bioinformatics* **26** 139–140.

Accepted Manuscript published as JOE-18-0493.R1. Accepted for publication: 30-Nov-2018

660 Roest HP, Baarends WM, de Wit J, van Klaveren JW, Wassenaar E, Hoogerbrugge JW, van
661 Cappellen WA, Hoeijmakers JHJ & Grootegoed JA 2004 The Ubiquitin-Conjugating DNA
662 Repair Enzyme HR6A Is a Maternal Factor Essential for Early Embryonic Development in
663 Mice. *Molecular and Cellular Biology* **24** 5485–5495.

664 Rotti PG, Xie W, Poudel A, Yi Y, Sun X, Tyler SR, Uc A, Norris AW, Hara M, Engelhardt JF *et*
665 *al.* 2018 Pancreatic and Islet Remodeling in Cystic Fibrosis Transmembrane Conductance
666 Regulator (CFTR) Knockout Ferrets. *The American Journal of Pathology* **188** 876–890.

667 Sauder KA, Hockett CW, Ringham BM, Glueck DH & Dabelea D 2017 Fetal overnutrition and
668 offspring insulin resistance and β-cell function: the Exploring Perinatal Outcomes among
669 Children (EPOCH) study. *Diabetic Medicine: A Journal of the British Diabetic Association*
670 **34** 1392–1399.

671 Schindelin J, Arganda-Carreras I, Frise E, Kaynig V, Longair M, Pietzsch T, Preibisch S,
672 Rueden C, Saalfeld S, Schmid B *et al.* 2012 Fiji: an open-source platform for biological-
673 image analysis. *Nature Methods* **9** 676–682.

674 Siddique T & Awan FR 2016 Effects of Reg3 Delta Bioactive Peptide on Blood Glucose Levels
675 and Pancreatic Gene Expression in an Alloxan-Induced Mouse Model of Diabetes.
676 *Canadian Journal of Diabetes* **40** 198–203.

677 Stull ND, Breite A, McCarthy R, Tersey SA & Mirmira RG 2012 Mouse islet of Langerhans
678 isolation using a combination of purified collagenase and neutral protease. *Journal of*
679 *Visualized Experiments: JoVE*. (doi:10.3791/4137)

680 Supek F, Bošnjak M, Škunca N & Šmuc T 2011 REVIGO summarizes and visualizes long lists
681 of gene ontology terms. *PloS One* **6** e21800.

682 Tam WH, Ma RCW, Ozaki R, Li AM, Chan MHM, Yuen LY, Lao TTH, Yang X, Ho CS, Tutino
683 GE *et al.* 2017 In Utero Exposure to Maternal Hyperglycemia Increases Childhood
684 Cardiometabolic Risk in Offspring. *Diabetes Care* **40** 679–686.

685 Vieleisis RA & Oh W 1983 Effect of increased substrate availability on fatty acid synthesis in the
686 growth retarded fetus. *Metabolism: Clinical and Experimental* **32** 90–94.

687 Wang J, Ma H, Tong C, Zhang H, Lawlis GB, Li Y, Zang M, Ren J, Nijland MJ, Ford SP *et al.*
688 2010 Overnutrition and maternal obesity in sheep pregnancy alter the JNK-IRS-1 signaling
689 cascades and cardiac function in the fetal heart. *The FASEB Journal* **24** 2066–2076.

690 Wang H, Xue Y, Wang B, Zhao J, Yan X, Huang Y, Du M & Zhu M-J 2014 Maternal obesity
691 exacerbates insulitis and type 1 diabetes in non-obese diabetic mice. *Reproduction* **148**
692 73–79.

693 White V, Jawerbaum A, Mazzucco MB, Gauster M, Desoye G & Hiden U 2015 Diabetes-
694 associated changes in the fetal insulin/insulin-like growth factor system are organ specific in
695 rats. *Pediatric Research* **77** 48–55.

696 Wu Y, Quan Y, Liu Y, Liu K, Li H, Jiang Z, Zhang T, Lei H, Radek KA, Li D *et al.* 2016
697 Hyperglycaemia inhibits REG3A expression to exacerbate TLR3-mediated skin
698 inflammation in diabetes. *Nature Communications* **7** 13393.

699 Xia F, Cao H, Du J, Liu X, Liu Y & Xiang M 2016 Reg3g overexpression promotes β cell
700 regeneration and induces immune tolerance in nonobese-diabetic mouse model. *Journal of*
701 *Leukocyte Biology* **99** 1131–1140.

702 Xiang L, Naik JS, Abram SR & Hester RL 2007 Chronic hyperglycemia impairs functional
703 vasodilation via increasing thromboxane-receptor-mediated vasoconstriction. *American*
704 *Journal of Physiology. Heart and Circulatory Physiology* **292** H231–H236.

705 Yao J, Wang C, Walsh SA, Hu S, Sawatzke AB, Dang D, Segar JL, Ponto LLB, Sunderland JJ
706 & Norris AW 2010 Localized fetomaternal hyperglycemia: spatial and kinetic definition by
707 positron emission tomography. *PloS One* **5** e12027.

708 Yokomizo H, Inoguchi T, Sonoda N, Sakaki Y, Maeda Y, Inoue T, Hirata E, Takei R, Ikeda N,
709 Fujii M *et al.* 2014 Maternal high-fat diet induces insulin resistance and deterioration of
710 pancreatic β-cell function in adult offspring with sex differences in mice. *American Journal*
711 *of Physiology. Endocrinology and Metabolism* **306** E1163–E1175.

712 Zambrano E, Sosa-Larios T, Calzada L, Ibáñez CA, Mendoza-Rodríguez CA, Morales A &
713 Morimoto S 2016 Decreased basal insulin secretion from pancreatic islets of pups in a rat
714 model of maternal obesity. *The Journal of Endocrinology* **231** 49–57.

715
716
717

 Accepted Manuscript published as JOE-18-0493.R1. Accepted for publication: 30-Nov-2018

Figure Legends

Figure 1. (A) Schematic representing localized fetomaternal hyperglycemia model. (B) Experimental timeline. Fetal pups were exposed to hyperglycemia from GD20 to 22, delivered via Cesarean section and cross-fostered to healthy dams. The cross-fostered pups were evaluated at weaning and at adulthood. (C) Maternal blood glucose was unchanged before (GD20) and during infusion (GD22) (left panel, n=13 mothers). During infusion, the glucose level in blood returning from the left uterine vein was higher than that of the right uterine vein (right panel, n=15 mothers). (D) The glucose levels of fetuses residing in left uterine horn (HG) were higher than those of their respective controls (Con) during glucose infusion while the placenta was intact (n=22-26 fetus from 12 mothers), but lower 30 minutes after birth (right panel, 12-14 pups from seven mothers). (E) Insulin levels of HG pups were higher as well (n=5 pups/group from five mothers). (F) Pancreatic beta- and alpha-cell area in the HG fetal pups (n = 5-6 pups/group from five mothers).

Figure 2. (A) Heatmap showing differentially expressed genes regulating diseases and biofunction predicted by IPA (n=3 fetal islet samples/group from three mothers; each islet samples prepared from pool of one pancreas from each gender). Left panel: 24 genes that enriched diabetes mellitus disease process (adjusted p-value = $2.43X10^{6}$). Right panel: Cell death process was upregulated by 41 genes (adjusted p-value = $2.38X10^{4}$). (B) Up- and down-regulated DEGs were analyzed separately using PANTHER and enriched GO BP was further summarized using REVIGO with the following parameters - database: whole UniProt; semantic similarity measure: Resnik; similarity allowed: Small (0.5). Note that up-regulated genes enriched immune and inflammatory processes (red circles) and down-regulated genes enriched different biological processes (blue circles). There were two commonly enriched GO BP (G4- response to stimulus, purple circle in C1 - immune responses/humoral immune response). The table on right shows the summarized list of GO biological processes (BP) and number/percentage of genes annotated to the GO BP.

Figure 3. Validation of RNA-seq results. (A) Graph correlating four down-regulated differentially expressed genes (from left-right: *Reg3g*: n=4 fetal islet samples/group, *Reg3b*: n=4 fetal islet samples/group, *Mmp7*: n=3 fetal islet samples/group, *Gabrp*: n=5 fetal islet samples /group) (one was technical replicate from RNA-seq experiment was included in *Reg3g*, *Reg3b* and *Gabrp*). (B) Graph showing consistent decrease in area positive for Reg3g in pancreatic beta cell area (Ins+) (*paired t-test $p<0.05$, each symbol represents an average data point obtained from three to five islets per sections, total of two sections per fetus, n=5 GD22 fetuses/group from five mothers). Internal pairs were connected with solid line. Image panel on right showing representative immunofluorescence images obtained from pancreatic tissue of Con and HG pups' pancreatic sections on the same slide.

Figure 4. HG weanlings developed glucose intolerance and pancreatic islet insulin secretory defect. (A) 1 g/kg intraperitoneal glucose tolerance testing showing increased blood glucose level at 10 timepoint, and (B) higher incremental glucose area under the curve (iAUC) (*$p<0.05$, n=7-10 male weanlings from six mothers, internal pairs were connected with dashed lines). (C) 2 g/kg intraperitoneal glucose tolerance testing yielded the same result where HG pups continued to have a higher glucose level at 10 min and (D) a higher incremental glucose AUC (*$p<0.05$, n=7-9 male weanlings/group from four mothers, internal pairs were connected with dashed lines). (E) Alamar blue cell viability assay showing the cell viability of HG islets was decreased (*$p<0.05$, 7-8 islets per replicate, n=4 pups/group from four mothers). (F) *Ex-vivo* static GSIS showing decreased HG islets insulin secretion at 5.6 mM glucose and 16.7 mM glucose phase. (*$p<0.05$, 20-25 islets/group collected from n=5 weanlings/group from five mothers). (G) Insulin tolerance testing of weanling males (n = 4-6 HG male/group from three mothers).

Figure 5. (A) 1 g/kg intraperitoneal glucose tolerance testing on two month old adult male offspring showing higher blood glucose level at 10 min timepoint and (B) higher incremental glucose iAUC (n=6-7 male/group, five mothers). (C) Serum insulin at 0, 10 and 30 min

 Accepted Manuscript published as JOE-18-0493.R1. Accepted for publication: 30-Nov-2018

timepoints during GTT showing decreased 10 min serum insulin level in HG male adult (n=4 males/group, four mothers, * $p<0.05$ when statistic was performed on fold change of insulin from baseline). (D) Graph showing consistent trend ($p=0.06$) of decrease in beta cell area across adult pancreatic sections, with a (E) decreased in pancreatic weight and ultimately decreased in (F) beta cell mass (n=4 males/group from four mothers). (G) Offspring weight from birth until adulthood (birth n=64-71 pups from 14 mothers; 7d/o n=7-14 pups from three mothers; 14d/o n=12-13 pups from three mothers; 21d/o n=17-19 males from six mothers; 2mo n=6-7 males from five mothers). (H) Fat to lean ratio of weanling (n=3-5 males/group from three mothers) and two month old adult showing no difference between Con and HG offspring (n=9-10 males from seven mothers).

Supplemental Figure Legends

Supplemental Figure 1: GD22 fetal pancreatic sections (n=3 pups/group from 3 mothers of independent infusions) were stained with the aforementioned anti-insulin Ab and DAPI, and the number of nuclei (DAPI) were counted and normalized to 1000 μm^2 insulin-positive area.

Supplemental Figure 2: 3 GD20 pregnant dams underwent the exact same surgery with saline infused into left uterine artery (SAL). Male pups were cross-fostered and GTT was performed on postnatal day 21 as described in the methods section. The glucose levels between 2 groups are analyzed using the same statistical approach as described in manuscript (two-way ANOVA tests followed by Bonferroni multiple comparison tests)

Supplemental Figure 3: Measurement of serum (A) Interferon-gamma, (B) Tnf-alpha, (C) Il-1B, (D) IL-17, and (E) Cxcl10 showing no difference between 2 groups. Each symbol represents one replicate with solid line connecting paired group (n=3-5/group, from three to five mothers). Serum was collected from fetal, neonatal, and adult offspring of Con and HG, then measured using Milliplex Rat Cytokine/Chemokine Magnet-ic Bead Panel - Immunology

Multiplex Assay (RECYTMAG-65K, Millipore Sigma, MA) by Indiana University Multiplex Analysis Core. This assay is designed to simultaneously quantify selected rat cyto-kines. The kit contains spectrally distinct antibody-immobilized beads, cytokine standard cocktail, streptavidin-phycoerythrin, assay buffer, wash buffer, serum matrix, and microtitre filter plate. Following the manufacturer's recommendation, 25 ul of samples were diluted (1 :2) and processed, then analyzed using Bio-Plex 200 System with High Throughput Fluidics (HTF) Multiplex Assay Array System (Bio-Rad Laboratories, Hercules, CA)> All the samples were run in duplicate. The detection limits for the measured cytokines are as follow: IFN-Gamma 6.2 pg/ml, TNF-Alpha 1.9 pg/ml, IL-1 B 2.8 pg/ml, IL-17 2.3 pg/ml, Cxcl10 1.4 pg/ml).

Accepted Manuscript published as JOE-18-0493.R1. Accepted for publication: 30-Nov-2018

Table 1: Primer sequences of target genes

Gene (Accession Number)		Sequence (5'-3')	Company
Reg3g	Fwd	TGTGCCCACTTCACGTATCA	IDT
(NM_173097.1)	Rev	GGATCATGGAGCCCAATCCA	
Reg3b	Fwd	GGAAACAGCTACCAATATACC	Sigma
(NM_053289.1)	Rev	CTCCATCTTAGAAATCCAGAAG	
Gabrp	Fwd	AGATGGCAGTCAAAGATAGG	Sigma
(NM_031029.1)	Rev	GTTTAAAGCTGGAGATGGAG	
Mmp7	Fwd	ACAGACTTGCCTCGGTTCTT	IDT
(NM_012864.2)	Rev	GTCTCCGTGATCTCCCCTTG	
Actb	Fwd	AGGTCATCACTATTGGCAACGA	Eurofins
(NM_031144.3)	Rev	CACTTCATGATGGATTGAATGTAGTT	

Table 2: Downregulated genes with known functions of pancreatic islets

Gene	FC	FDR	Expression	Pancreatic Islet				References
				Early Development	Regeneration/ Anti-apoptotic	Inflammation	Insulin Secretion	
Reg3g	-24.3	4.29E-08	Neonatal & adult	Yes	Yes	Yes	Yes	(Gagliardino et al. 2003; Petropavlovskaia et al. 2006; Assouline-Thomas et al. 2015;
Reg3b	-7.7	5.14E-03	Neonatal & adult	Yes	Yes	Yes	Yes	Barbosa et al. 2006; Madrid et al. 2013; Gagliardino et al. 2003; Assouline-Thomas et al. 2015; Siddique and Awan 2016; Xia et al. 2016)
Ctgf	-1.8	1.34E-02	Embryonic & pregnancy	Yes	Yes	Unknown	Yes	(Crawford et al. 2009; Pasek et al. 2017; Riley et al. 2015)
Fgfr3	-2.0	2.91E-02	Embryonic	Yes	Yes	Unknown	Unknown	(Arnaud-Dabernat et al. 2007)
Clu	-2.0	3.44E-03	Embryonic & neonatal	Unknown	Yes	Yes	Unknown	(Kaya-Dagistanli and Ozturk 2013)
Mmp7	-4.7	7.05E-03	Neonatal	No	Yes	Unknown	No	(Nishihama et al. 2018; Perez et al. 2005)
Gabrp	-3.0	1.22E-03	Unknown	Unknown	Yes	Unknown	Yes	(Wang et al. 2014; Prud'homme et al. 2014)
IL17rb	-2.6	1.71E-02	Unknown	Unknown	Yes	Yes	Unknown	(Yaochite et al. 2013)
Cftr	-2.9	5.73E-03	Neonatal & adult	Yes	Unknown	Unknown	Yes	(Hart et al 2018; Rotti et al 2018)

Accepted Manuscript published as JOE-18-0493.R1. Accepted for publication: 30-Nov-2018

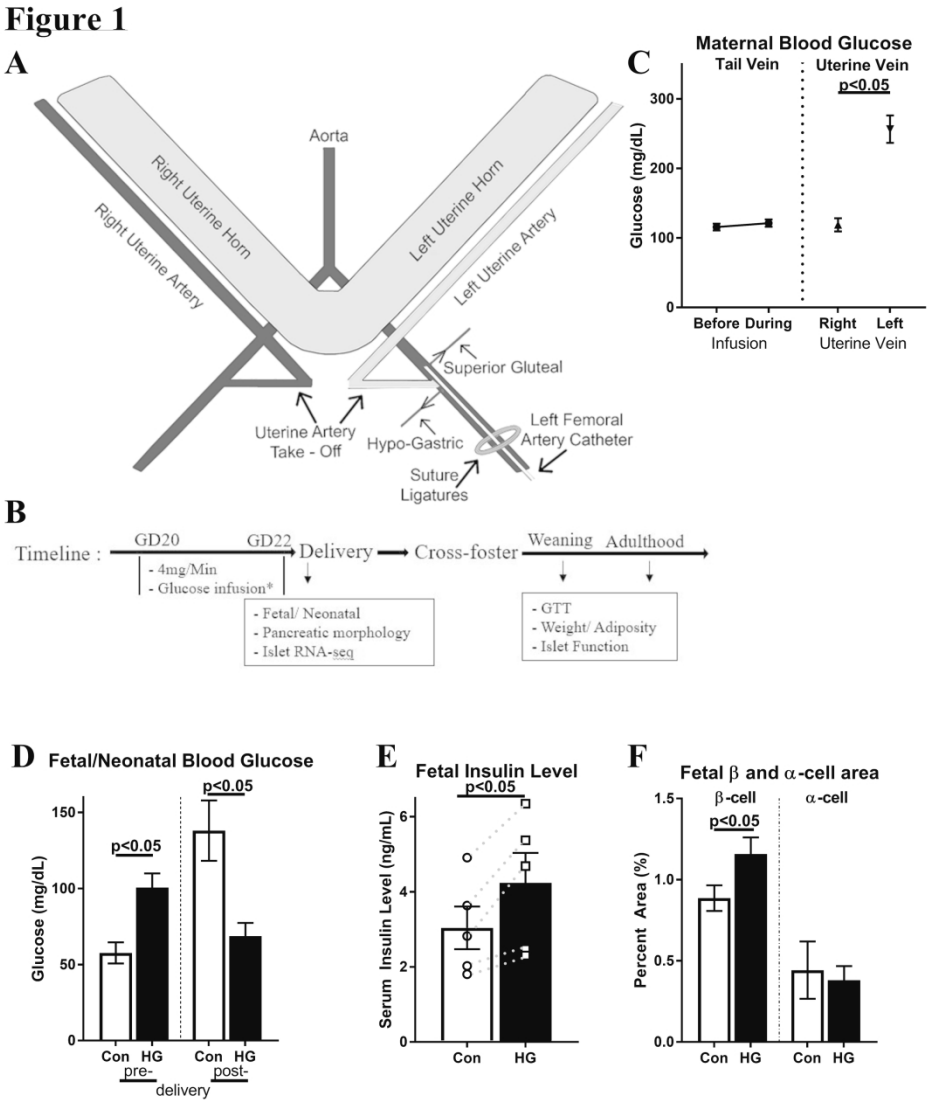

Figure 1. (A) Schematic representing localized fetomaternal hyperglycemia model. (B) Experimental timeline. Fetal pups were exposed to hyperglycemia from GD20 to 22, delivered via Cesarean section and cross-fostered to healthy dams. The cross-fostered pups were evaluated at weaning and at adulthood. (C) Maternal blood glucose was unchanged before (GD20) and during infusion (GD22) (left panel, n=13 mothers). During infusion, the glucose level in blood returning from the left uterine vein was higher than that of the right uterine vein (right panel, n=15 mothers). (D) The glucose levels of fetuses residing in left uterine horn (HG) were higher than those of their respective controls (Con) during glucose infusion while the placenta was intact (n=22-26 fetus from 12 mothers), but lower 30 minutes after birth (right panel, 12-14 pups from seven mothers). (E) Insulin levels of HG pups were higher as well (n=5 pups/group from five mothers). (F) Pancreatic beta- and alpha-cell area in the HG fetal pups (n = 5-6 pups/group from five mothers).

239x274mm (300 x 300 DPI)

Figure 2

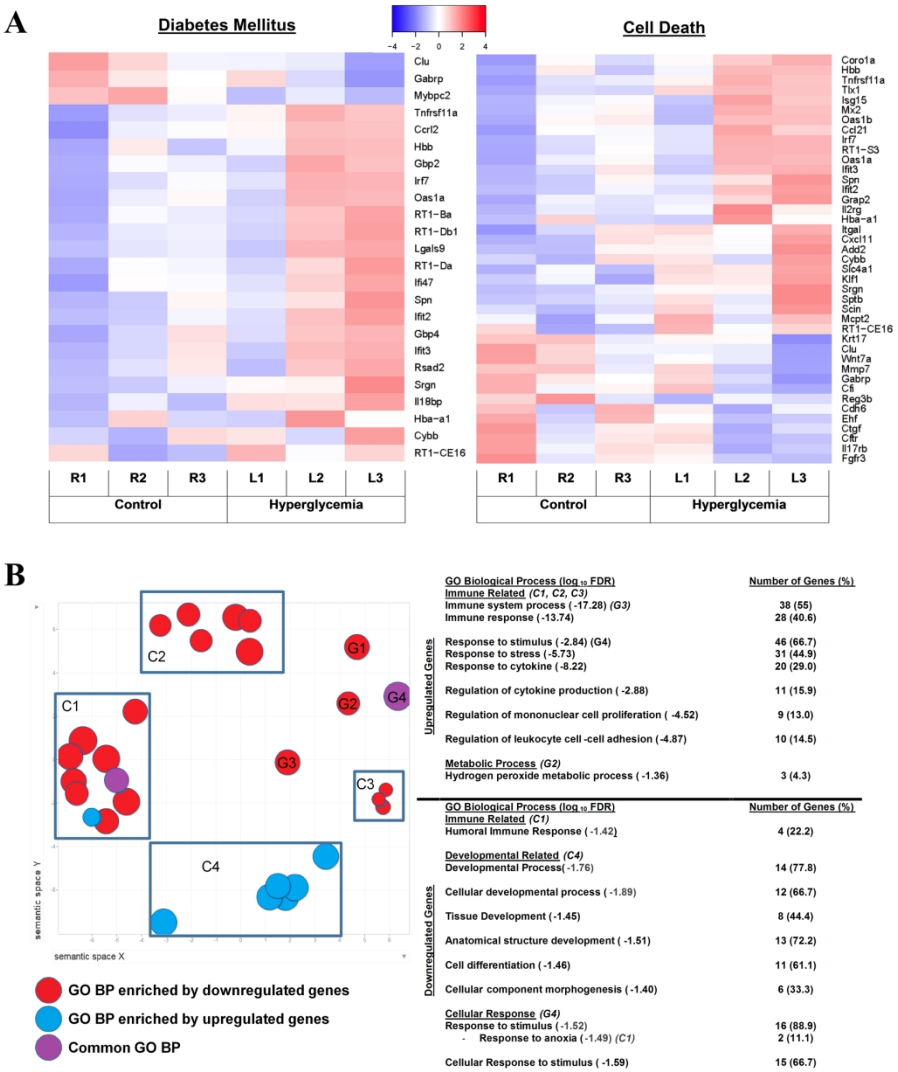

Figure 2. (A) Heatmap showing differentially expressed genes regulating diseases and biofunction predicted by IPA. Left panel: 24 genes that enriched diabetes mellitus disease process (adjusted p-value = 2.43X10^6). Right panel: Cell death process was upregulated by 41 genes (adjusted p-value = 2.38X10^4). (B) Up- and down-regulated DEGs were analyzed separately using PANTHER and enriched GO BP was further summarized using REVIGO with the following parameters - database: whole UniProt; semantic similarity measure: Resnik; similarity allowed: Small (0.5). Note that up-regulated genes enriched immune and inflammatory processes (red circles) and down-regulated genes enriched different biological processes (blue circles). There were two commonly enriched GO BP (G4- response to stimulus, purple circle in C1 - immune responses/humoral immune response). The table on right shows the summarized list of GO biological processes (BP) and number/percentage of genes annotated to the GO BP.

245x279mm (300 x 300 DPI)

Accepted Manuscript published as JOE-18-0493.R1. Accepted for publication: 30-Nov-2018

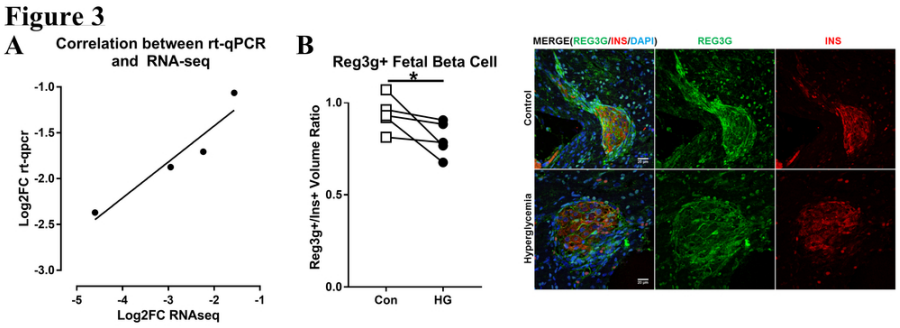

Figure 3. Validation of RNA-seq results. (A) Graph correlating four down-regulated differentially expressed genes (from left-right: Reg3g, Reg3b, Mmp7, Gabrp) (n = 3-5 pups/group from three to five independent set of experiments, which one was technical replicate from RNA-seq experiment). (B) Graph showing consistent decrease in area positive for Reg3g in pancreatic beta cell area (Ins+) (*paired t-test $p<0.05$, each symbol represents an average data point obtained from three to five islets per sections, total of two sections per fetus, n=5 GD22 fetuses/group from five mothers). Internal pairs were connected with solid line. Image panel on right showing representative immunofluorescence images obtained from pancreatic tissue of Con and HG pups' pancreatic sections on the same slide.

93x34mm (300 x 300 DPI)

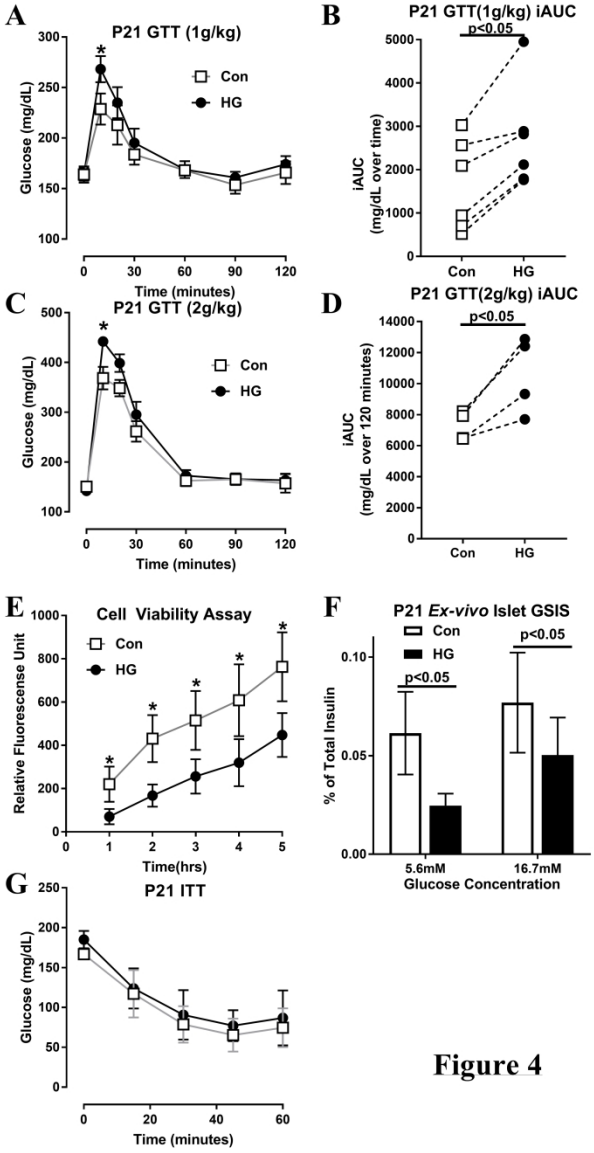

Figure 4

Figure 4. HG weanlings developed glucose intolerance and pancreatic islet insulin secretory defect. (A) 1 g/kg intraperitoneal glucose tolerance testing showing increased blood glucose level at 10 timepoint, and (B) higher incremental glucose area under the curve (iAUC) (*p<0.05, n=7-10 male weanlings from six mothers, internal pairs were connected with dashed lines). (C) 2 g/kg intraperitoneal glucose tolerance testing yielded the same result where HG pups continued to have a higher glucose level at 10 min and (D) a higher incremental glucose AUC (*p<0.05, n=7-9 male weanlings/group from four mothers, internal pairs were connected with dashed lines). (E) Alamar blue cell viability assay showing the cell viability of HG islets was decreased (*p<0.05, 7-8 islets per replicate, n=4 pups/group from four mothers). (F) Ex-vivo static GSIS showing decreased HG islets insulin secretion at 5.6 mM glucose and 16.7 mM glucose phase. (*p<0.05, 20-25 islets/group collected from n=5 weanlings/group from five mothers). (G) Insulin tolerance testing of weanling males (n = 4-6 HG male/group from three mothers)

281x509mm (300 x 300 DPI)

Accepted Manuscript published as JOE-18-0493.R1. Accepted for publication: 30-Nov-2018

Figure 5

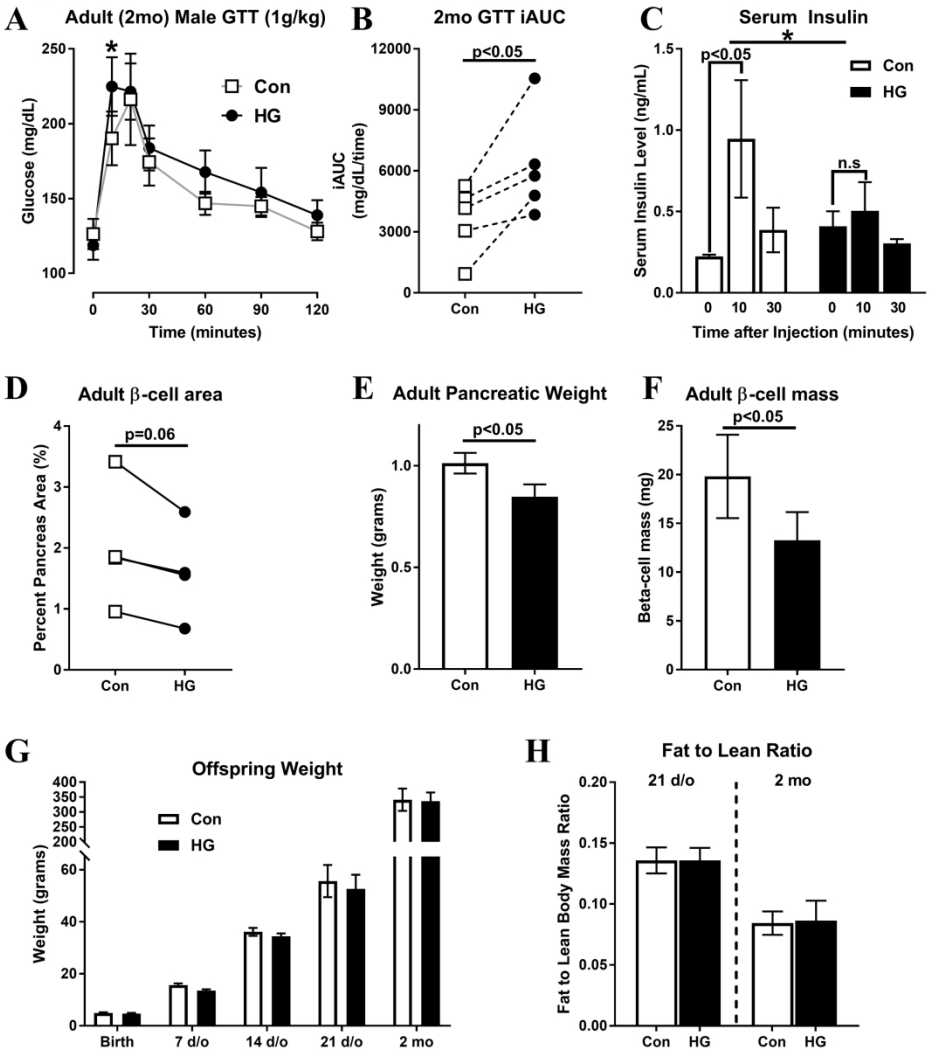

Figure 5. (A) 1 g/kg intraperitoneal glucose tolerance testing on two month old adult male offspring showing higher blood glucose level at 10 min timepoint and (B) higher incremental glucose iAUC (n=6-7 male/group, five mothers). (C) Serum insulin at 0, 10 and 30 min timepoints during GTT showing decreased 10 min serum insulin level in HG male adult. (n=4 males/group, four mothers, * $p<0.05$ when statistic was performed on fold change of insulin from baseline). (D) Graph showing consistent trend ($p=0.06$) of decrease in beta cell area across adult pancreatic sections, with a (E) decreased in pancreatic weight and ultimately decreased in (F) beta cell mass (n=4 males/group from four mothers). (G) Offspring weight from birth until adulthood (birth n=64-71 pups from 14 mothers; 7d/o n=7-14 pups from three mothers; 14d/o n=12-13 pups from three mothers; 21d/o n=17-19 males from six mothers; 2mo n=6-7 males from five mothers). (H) Fat to lean ratio of weanling (n=3-5 males/group from three mothers) and two month old adult showing no difference between Con and HG offspring (n=9-10 males from seven mothers).

237x271mm (300 x 300 DPI)

Accepted Manuscript published as JOE-18-0493.R1. Accepted for publication: 30-Nov-2018

Supp Fig 1: Number of Cells (DAPI) in INS+ area (1000µm2)

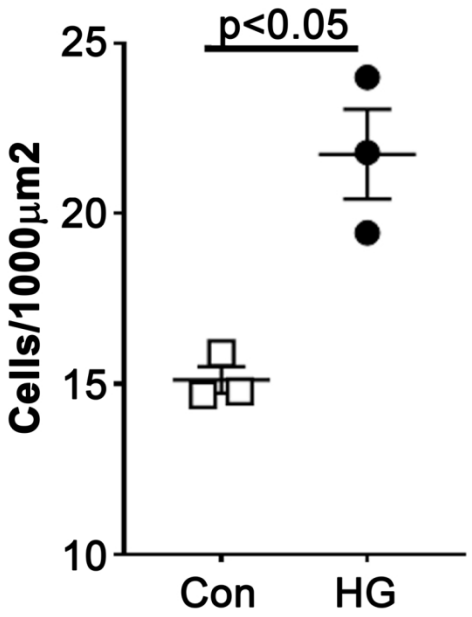

152x177mm (300 x 300 DPI)

Supp Fig 2: GTT of left uterine horn pups infused with 48hours of saline (Sal) from GD20 to 22 vs right uterine horn controls (Con)

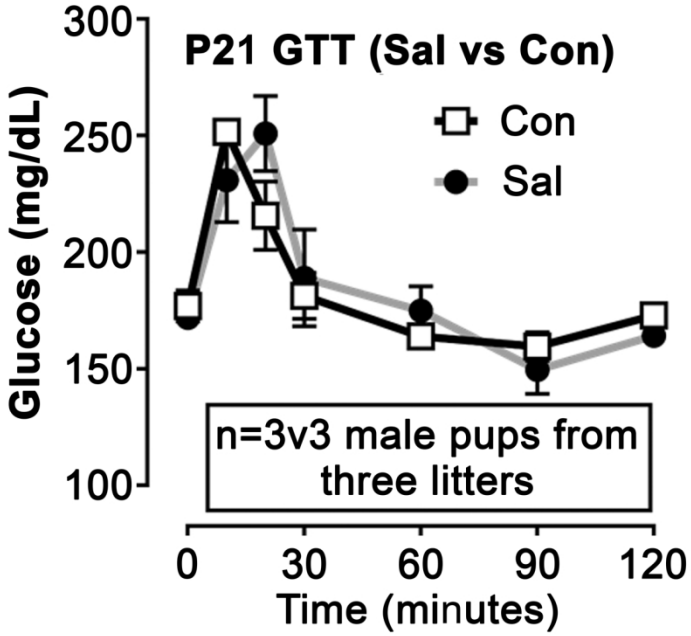

152x165mm (300 x 300 DPI)

Accepted Manuscript published as JOE-18-0493.R1. Accepted for publication: 30-Nov-2018

Supp Fig 3: Inflammatory cytokines in fetal, neonatal and adult offspring

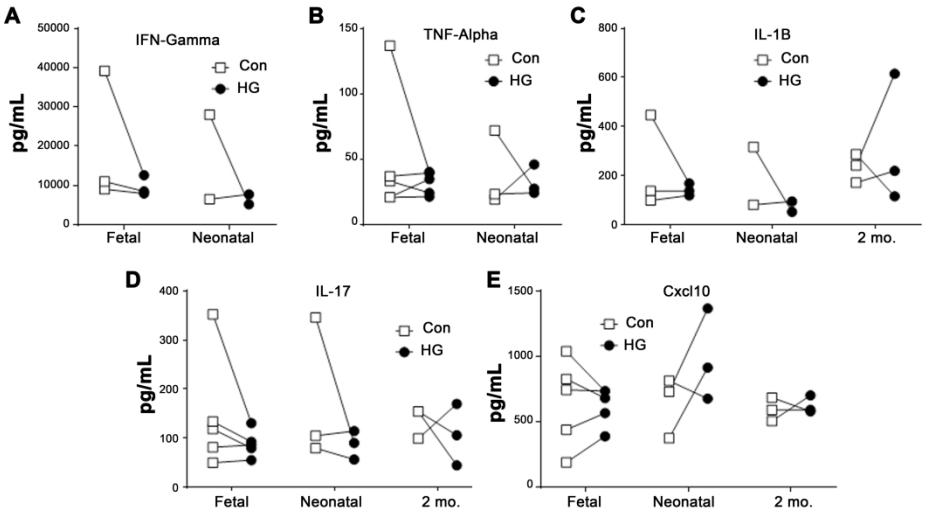

279x215mm (300 x 300 DPI)

Supp Table 1: List of Differentially expressed genes in HG GD22 islets

Symbol	Gene Name	Fold Change	FDR
Slc4a1	solute carrier family 4 (anion exchanger), member 1	25.07	9.43E-04
Ahsp	alpha hemoglobin stabilizing protein	13.29	2.22E-03
Lgals5	lectin, galactose binding, soluble 5	9.76	3.09E-04
Alas2	5'-aminolevulinate synthase 2	9.68	1.06E-05
Cd52	CD52 molecule	7.37	1.71E-05
Klf1	Kruppel like factor 1	7.31	3.90E-02
Shisa3	shisa family member 3	7.00	1.58E-05
Ptprcap	protein tyrosine phosphatase, receptor type, C-associated protein	6.34	7.43E-04
Nfe2	nuclear factor, erythroid 2	6.24	7.39E-05
RT1-Ba	RT1 class II, locus Ba	6.17	8.82E-05
RT1-Da	RT1 class II, locus Da	5.33	4.43E-03
Mx1	myxovirus (influenza virus) resistance 1	5.24	2.31E-08
Sptb	spectrin, beta, erythrocytic	5.16	1.47E-02
Adgrg5	adhesion G protein-coupled receptor G5	5.14	3.94E-03
RT1-Db1	RT1 class II, locus Db1	4.59	3.11E-03
Hbb	hemoglobin subunit beta	4.50	2.04E-06
Tifab	TIFA inhibitor	4.32	1.39E-02
LOC100134871	beta globin minor gene	4.23	1.65E-03
Ifit3	interferon-induced protein with tetratricopeptide repeats 3	4.20	5.58E-03
Grap2	GRB2-related adaptor protein 2	4.13	2.91E-02
Irf7	interferon regulatory factor 7	3.88	2.97E-08
Napsa	napsin A aspartic peptidase	3.79	4.48E-02
Scin	scinderin	3.76	9.44E-03
Isg15	ISG15 ubiquitin-like modifier	3.70	3.44E-03
Rsad2	radical S-adenosyl methionine domain containing 2	3.60	2.91E-02
Traf3ip3	TRAF3 interacting protein 3	3.47	2.91E-02

Accepted Manuscript published as JOE-18-0493.R1. Accepted for publication: 30-Nov-2018

Symbol	Gene Name	Fold Change	FDR
Oas1a	2'-5' oligoadenylate synthetase 1A	3.41	3.77E-04
Gbp4	guanylate binding protein 4	3.40	3.45E-02
Cst7	cystatin F	3.36	8.66E-03
Ccrl2	C-C motif chemokine receptor like 2	3.31	1.34E-02
Mx2	MX dynamin like GTPase 2	3.30	1.47E-02
Gbp5	guanylate binding protein 5	3.19	9.43E-04
Srgn	serglycin	3.19	1.25E-03
Lgals9	galectin 9	3.11	2.50E-02
Gpr183	G protein-coupled receptor 183	3.06	8.66E-03
RT1-CE16	RT1 class I, locus CE16	3.04	6.23E-04
Spn	sialophorin	3.02	3.40E-02
Slc9a2	solute carrier family 9 member A2	2.99	3.40E-02
Cmpk2	cytidine/uridine monophosphate kinase 2	2.86	2.34E-03
Tmcc2	transmembrane and coiled-coil domain family 2	2.86	2.83E-02
Tox2	TOX high mobility group box family member 2	2.83	4.91E-02
Tlx1	T-cell leukemia, homeobox 1	2.82	1.22E-03
Fam46c	family with sequence similarity 46, member C	2.81	7.94E-04
Ifi27l2b	interferon, alpha-inducible protein 27 like 2B	2.81	2.63E-07
Add2	adducin 2	2.79	2.83E-02
Tnfrsf11a	TNF receptor superfamily member 11A	2.76	2.44E-02
Hba-a1	hemoglobin alpha, adult chain 1	2.71	4.98E-03
Ccl21	C-C motif chemokine ligand 21	2.69	2.73E-05
Itgal	integrin subunit alpha L	2.62	2.91E-02
Cfp	complement factor properdin	2.61	2.83E-02
Mcpt2	mast cell protease 2	2.60	2.89E-02
Oas1b	2-5 oligoadenylate synthetase 1B	2.58	2.77E-02
RT1-S3	RT1 class Ib, locus S3	2.49	2.54E-04
Il18bp	interleukin 18 binding protein	2.45	3.27E-02

Symbol	Gene Name	Fold Change	FDR
Slamf9	SLAM family member 9	2.43	1.47E-02
Cxcl11	C-X-C motif chemokine ligand 11	2.43	3.85E-02
Coro1a	coronin 1A	2.42	2.34E-03
Slc28a2	solute carrier family 28 member 2	2.42	3.80E-02
Cybb	cytochrome b-245 beta chain	2.37	8.66E-03
Ifit2	interferon-induced protein with tetratricopeptide repeats 2	2.34	7.99E-03
Apol3	apolipoprotein L, 3	2.27	3.86E-03
Ifi47	interferon gamma inducible protein 47	2.11	1.86E-02
Gbp2	guanylate binding protein 2	2.11	3.04E-03
Il2rg	interleukin 2 receptor subunit gamma	2.07	4.23E-02
Fbln5	fibulin 5	2.07	4.50E-02
Fmnl1	formin-like 1	2.06	4.39E-02
Bst2	bone marrow stromal cell antigen 2	2.02	1.47E-02
Cldn5	claudin 5	1.84	2.60E-02
Tmem176a	transmembrane protein 176A	1.74	4.39E-02
Ctgf	connective tissue growth factor	-1.83	1.34E-02
Clu	clusterin	-2.01	3.44E-03
Fgfr3	fibroblast growth factor receptor 3	-2.01	2.91E-02
Sorbs2	sorbin and SH3 domain containing 2	-2.02	8.66E-03
Wnt7a	wingless-type MMTV integration site family, member 7A	-2.20	9.14E-03
Cdh6	cadherin 6	-2.28	2.77E-02
Ehf	ets homologous factor	-2.30	3.91E-02
Krt17	keratin 17	-2.31	3.96E-04
Dcdc2	doublecortin domain containing 2	-2.31	2.40E-02
Cfi	complement factor I	-2.57	3.67E-02
Il17rb	interleukin 17 receptor B	-2.63	1.71E-02
Cftr	cystic fibrosis transmembrane conductance regulator	-2.90	5.73E-03
Gabrp	gamma-aminobutyric acid type A receptor pi subunit	-2.95	1.22E-03

Accepted Manuscript published as JOE-18-0493.R1. Accepted for publication: 30-Nov-2018

Symbol	Gene Name	Fold Change	FDR
Mybpc2	myosin binding protein C, fast-type	-3.77	5.58E-03
Dmbt1	deleted in malignant brain tumors 1	-3.84	2.75E-03
Mmp7	matrix metallopeptidase 7	-4.71	7.05E-03
Reg3b	regenerating family member 3 beta	-7.72	5.14E-03
Reg3g	regenerating family member 3 gamma	-24.29	4.29E-08

Accepted Manuscript published as JOE-18-0493.R1. Accepted for publication: 30-Nov-2018

Supp Table 2: Pathways enriched by IPA

Ingenuity Canonical Pathways	-log (p-value)	zScore
Th1 Pathway	3.72E-02	1.341641
PKCθ Signaling in T Lymphocytes	7.42E-03	1.632993
iCOS-iCOSL Signaling in T Helper Cells	1.02E-04	1.889822
Neuroinflammation Signaling Pathway	5.63E-03	1.889822
Interferon Signaling	2.35E-03	2
Calcium-induced T Lymphocyte Apoptosis	2.63E-02	2
B Cell Development	5.50E-05	-
Antigen Presentation Pathway	7.25E-05	-
Autoimmune Thyroid Disease Signaling	2.40E-04	-
Graft-versus-Host Disease Signaling	2.40E-04	-
Crosstalk between Dendritic Cells and Natural Killer Cells	2.57E-04	-
IL-4 Signaling	2.57E-04	-
Th2 Pathway	3.89E-04	-
Th1 and Th2 Activation Pathway	1.55E-03	-
T Helper Cell Differentiation	1.95E-03	-
CD28 Signaling in T Helper Cells	2.57E-03	-
Allograft Rejection Signaling	4.08E-03	-
Altered T Cell and B Cell Signaling in Rheumatoid Arthritis	5.38E-03	-
OX40 Signaling Pathway	5.76E-03	-
Type I Diabetes Mellitus Signaling	1.48E-02	-
Nur77 Signaling in T Lymphocytes	1.70E-02	-
Leukocyte Extravasation Signaling	3.47E-02	-

Supp Table 3: EnrichR Analysis of downregulated genes

Term (Human Tissue from BioGPS)	P-value	Adjusted P-value	Combined Score
Pancreatic Islet	0.000173	0.003636	12.17
colon	0.022137	0.090228	6.74
Cardiac Myocytes	0.024595	0.090228	6.69
Trachea	0.001884	0.01978	6.10
Bronchial Epithelial Cells	0.025779	0.090228	5.49
Smooth Muscle	0.041504	0.124512	4.25

Term (Mouse Tissue from BioGPS)	P-value	Adjusted P-value	Combined Score
pancreas	0.020739	0.165911	8.42
intestine_small	0.007904	0.165911	7.72
thymocyte_SP_CD4+	0.014095	0.165911	7.57
cornea	0.055549	0.333291	4.98